HOSTED BY

ELSEVIER

Available online at www.sciencedirect.com

ScienceDirect

Soils and Foundations 62 (2022) 101204

SOILS AND FOUNDATIONS

www.elsevier.com/locate/sandf

Technical Paper

Bearing capacity evaluation of small-diameter spiral piles in soft ground subjected to combined loads

Hamidou Hamadoum Tamboura [a,*], Ryo Yamauchi [b], Koichi Isobe [c]

[a] *Laboratory of Analytical Geomechanics, Division of Civil Engineering, Graduate School of Engineering, Hokkaido University, Japan, Kita 13, Nishi 8, Kita-Ku, Sapporo, Hokkaido, 060-8628, JAPAN*

[b] *Materials Research Team, Cold-Region Maintenance Engineering Research Group, Civil Engineering Research Institute for Cold Region, Japan, 1-34 Hiragishi 1-jo 3-chome, Toyohira-ku, Sapporo, Hokkaido, 062-8602, JAPAN*

[c] *Laboratory of Analytical Geomechanics, Division of Civil Engineering, Graduate School of Engineering, Hokkaido University, Japan, Kita 13, Nishi 8, Kita-Ku, Sapporo, Hokkaido, 060-8628, JAPAN*

Received 14 April 2022; received in revised form 30 June 2022; accepted 25 July 2022

Abstract

In the current practices, the evaluation method for the bearing capacity of small-diameter spiral piles is a conservative method performed on the safe side, since it does not consider the integration effect with the surrounding ground due to rotational press-fitting. In addition, the evaluation method for the bearing capacity of spiral piles subjected to combined loads has not been established. In this study, a series of push-in, pull-out, and horizontal loading tests on spiral piles constructed on a soft viscous ground is conducted, and a method to easily consider the integration effect of the surrounding ground by rotational press-fitting is proposed. Subsequently, based on the proposed method, small-diameter spiral piles are modelled with a FEM analysis, various test results are reproduced, and coefficients for considering the integration effect of the surrounding ground in a numerical analysis are established. With the same FEM analysis method, using the established coefficients, the bearing capacity characteristics of vertical and batter spiral piles for combined loads are obtained. Finally, based on the results, formulas for the bearing capacity envelopes in the H-V-M space are proposed and the accuracy of the formulas are verified.

Keywords: Spiral pile; FEM analysis; Combined load; Failure envelope

1. Introduction

The construction of photovoltaic power generation facilities has been increasing along with the rising demand for renewable energy. Many solar power generation facilities have been constructed on sites with poor ground and construction conditions. To ensure the feasibility of the solar power generation business, increasing numbers of constructions have been carried out for such facilities. The constructions include large-scale ones on relatively inexpensive land with poor conditions and those on slopes. Conventionally, the major type of foundation used for photovoltaic power generation equipment is the concrete shallow foundation. However, with the above-mentioned constructions on a soft ground with poor conditions in mind, the development of new types of foundations using small-diameter and short steel pipe piles, spiral piles, and batter piles has been progressing in Japan (Araki 2013; Hirata et al. 2005; Sato et al. 2015). Compressive, horizontal, and uplift loads and moments generally act on these

Peer review under responsibility of The Japanese Geotechnical Society.

* Corresponding author.

E-mail addresses: hamidoutamboura@eis.hokudai.ac.jp (H.H. Tamboura), yamauchi-r@ceri.go.jp (R. Yamauchi), kisobe@eng.hokudai.ac.jp (K. Isobe).

https://doi.org/10.1016/j.sandf.2022.101204

piles simultaneously due to the actions of wind, earthquakes, landslides, etc. Many studies have reported the behaviour of other types of piles under combined loading: compressive-lateral loading (Meyerhof 1981; Meyerhof et al. 1983; Jain et al. 1987; Gotman 2000; Zhang and Small 2000; Small and Zhang, 2002; Johnson 2005; Abdel-Rahman and Achmus 2006; Karthigeyan et al. 2006, 2007; Achmus and Thieken 2010; Suleiman et al. 2010; Ashour et al. 2020) and lateral-uplift loading (Das et al. 1976; Ismael 1989; Darr et al. 1990; Rao and Prasad 1993; Mroueh and Shahrour 2007, 2009; Suits et al. 2012; Ayothiraman and Reddy 2014; Reddy and Ayothiraman 2015; Ashour et al. 2020). However, only a very limited number of studies have reported the behaviour of spiral piles under combined loading.

The spiral pile is an advantageous pile type because it has high resistance to vertical loads (push-in and pull-out loads). On the other hand, its disadvantage is its low flexural rigidity, namely, its horizontal resistance is lower than that of the steel pipe pile of the same diameter. When the conventional design method in Japan, which uses 1 % of the pile diameter (lower limit: 15 mm) as the allowable displacement, is applied to small-diameter piles, the possibility of resulting in overdesign exists. This is because the elastic ground reaction force method, which is generally used in the pile foundation design, overestimates the horizontal displacement of these small-diameter piles. In addition, the high resistance to the vertical load of spiral piles is due to the effect of its integration with the surrounding ground generated during rotational press-fitting. However, in many cases, the design takes the safe side without considering this integration effect from the rotational press-fitting. Therefore, it is necessary to properly evaluate the bearing capacity characteristics of small-diameter spiral piles and to produce more rational designs.

In the conventional design, allowable values are set for the vertical and horizontal load directions, and individual evaluations are performed separately. In reality, however, combined horizontal and vertical loads act on the structure due to the actions of wind load, landslides, etc. The bearing capacity against the combined vertical and horizontal loads may be lower than the bearing capacity evaluated independently. The spiral pile is also expected to be used as an anchor by taking advantage of its excellent pull-out resistance. However, since only the pull-out resistance is considered in the conventional anchor design, it is extremely important to evaluate the bearing capacity performance against the combined pull-out and horizontal loads and to design the spiral pile anchors rationally for slope stabilization. In this way, it is thought that an appropriate evaluation of the bearing capacity of small-diameter piles against combined loads will lead to the rational design of small-diameter pile foundations and anchors. In addition, under such combined loading conditions, it is common to use the H-V-M (horizontal, vertical, and moments) failure surfaces/envelopes to assess the foundation's capacity to withstand these conditions.

In this study, a series of push-in, pull-out, and horizontal loading tests is conducted on spiral piles constructed on a soft viscous ground, and a method is proposed to simply consider the integration effect between rotationally press-fit spiral piles and the surrounding ground. Next, based on the proposed method, small-diameter spiral piles are modelled in FEM analyses, the physical test results are reproduced, and some additional parameters necessary for the numerical analysis are identified. Using the identified parameters, the bearing capacity characteristics of vertical and batter spiral piles under combined loads are obtained by the same analysis method. Finally, based on the results, formulas for the bearing capacity envelopes in the H-V-M space are proposed for both vertical and batter spiral piles.

2. OUTLINE OF LOADING tests

Fig. 1 shows a schematic of the model spiral pile used in this study. The pile is manufactured by the twisting of a flat steel bar (SS400), and its features are as follows:

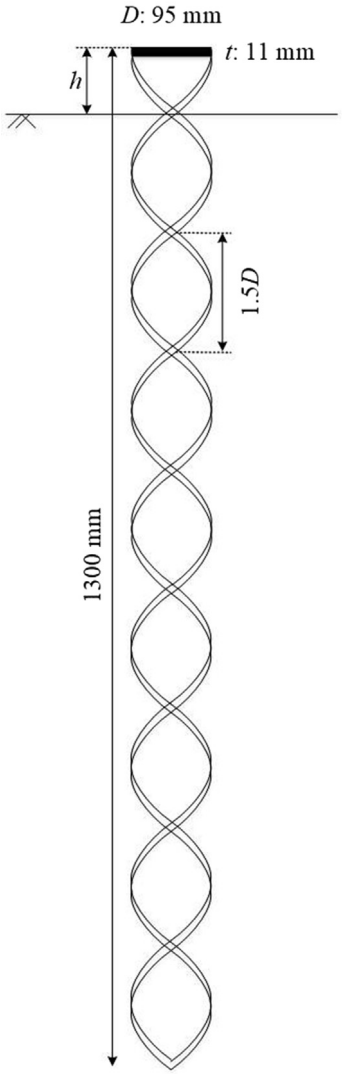

Fig. 1. Schematic of spiral pile.

a) Construction can be done manually by applying rotational force to press-fit each pile and controlling the amount of penetration per rotation so as to minimize the disturbance to the surrounding ground.
b) The effect of the integration between the pile and the surrounding ground can be expected by rotational press-fitting, which increases the push-in and pull-out load capacities.
c) By rotating the pile in the ground in the reverse direction, it can be easily pulled out and reused. The pile has high workability and a less time-consuming installation process.

As shown in Fig. 1 and Table 1, the pile measures 1.3 m in length, 95 mm in external diameter, and 11 mm in plate thickness.

In the tests in this study, spiral piles were rotationally press-fitted into a cement-improved soft viscous ground (average N value: 3.9 and uniaxial compressive strength: 58.5 kPa), and pure push-in, pure pull-out, and pure horizontal loading tests were performed following JGS (the Japanese Geotechnical Society) standards JGS 1811–2002 (Method for Static Axial Compressive Load Test of Single Piles), JGS 1813–2002 (Method for Static Axial Tensile Load Test of Single Piles), and JGS 1831–2010 (Horizontal load test of piles), respectively. Each loading test was carried out with protrusion lengths (h) of 50 mm, 100 mm, and 150 mm. The loads were applied using a hydraulic jack. Fig. 2 shows the test device in the case of pure horizontal loading.

3. EXPERIMENTAL results

Fig. 3 shows the relationship between the load and the displacement obtained in each test, where the pull-out load and the push-in load are considered as a positive load and a negative load, respectively. h50, h100, and h150 represent the tests with loading heights (h) of 50 mm, 100 mm, and 150 mm, respectively. (The loading height here is the distance from the loading point to the ground surface). Some tests were conducted twice with the same loading height (for example, h100-1 and h100-2). For the vertical load, the ultimate load capacity is interpreted using the double tangent method, as suggested by Shanker et al. (2007) and used by Reddy and Ayothiraman (2015). The equation of the conventional vertical (push-in and pull-out) bearing capacity is presented by **Eq. (1),** and the conventional horizontal resistance of the pile can be obtained by Chang's equation, **Eq. (2)**. The test results in Fig. 3 show that the push-in and pull-out bearing capacities calculated with **Eq. (1)** and the horizontal resistance calculated with **Eq. (2)** both underestimate the actual capacity of the spiral pile. This underestimation is caused by the fact that neither equation considers the impact of the integration of the surrounding ground generated by the rotational press-fitting, namely, the direct consequence of an apparent increase in pile diameter, the increase in strength of the ground immediately below the pile tip, and the increase in flexural rigidity of the pile, as illustrated in Fig. 4.

Table 1
Properties of spiral pile.

Material		Steel SS400
Length	m	1.3
External diameter	mm	95
Plate thickness	mm	11
Young's modulus	kN/m^2	2.05x10^8

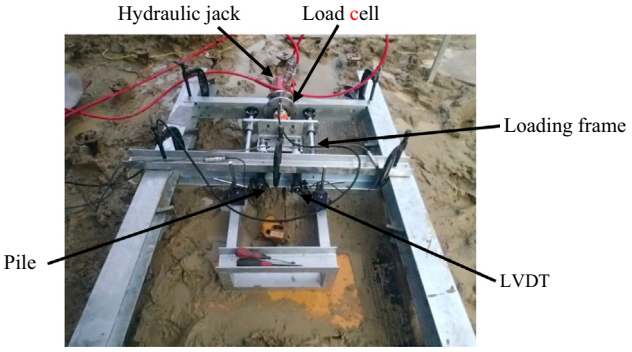

Fig. 2. Horizontal loading test device.

In this study, the bearing capacity equation (**Eq. (1)**) and Chang's equation (**Eq. (2)**) were adapted to spiral piles by using correction coefficients ξ, η, and ζ for the apparent increase in pile diameter, the increase in strength of the ground immediately below the pile tip, and the increase in flexural rigidity of the pile, respectively. After the correction, the integration effect was considered without complicated procedures, using **Eqs. (3) to (6)**. Since variations are observed in the experimental results, the minimum value of the correction coefficient obtained from each test was used as the representative value for the sake of safety. The obtained correction coefficients are $\xi = 1.99$, $\eta = 0.73$, and $\zeta = 1.94$. These correction coefficients depend on the pile size, spiral shape, and characteristics of the surrounding ground. However, for small-diameter spiral piles in clayey soil, the application of the coefficients is generally useful, including practical cases. The vertical bearing capacities and horizontal load – horizontal displacement relationship obtained with the corrected equations are plotted in Fig. 3. The load capacities given by these corrected equations roughly correspond to displacements equivalent to 10 % of the pile diameter in the experiment.

$$R_u = q_p A_p + \tau_c L_c \phi \tag{1}$$

$$y_t = \frac{(1+\beta h)^3 + 1/2}{3EI\beta^3} H + \frac{(1+\beta h)^2}{2EI\beta^2} M \tag{2}$$

$$A'_p = \frac{\pi(\xi D)^2}{4} \tag{3}$$

$$q'_p = 3\eta q_u = 3\eta(15N) \tag{4}$$

$$\phi' = \pi \xi D \tag{5}$$

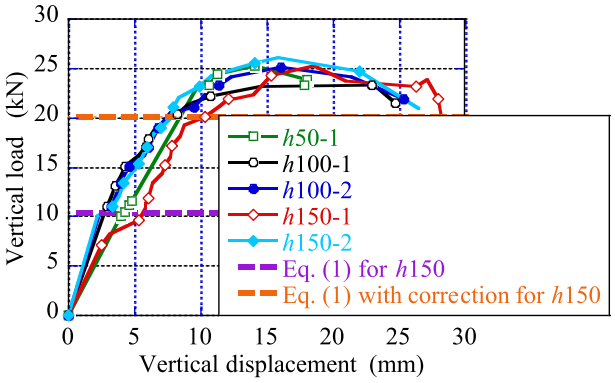

(a) Pull-out tests

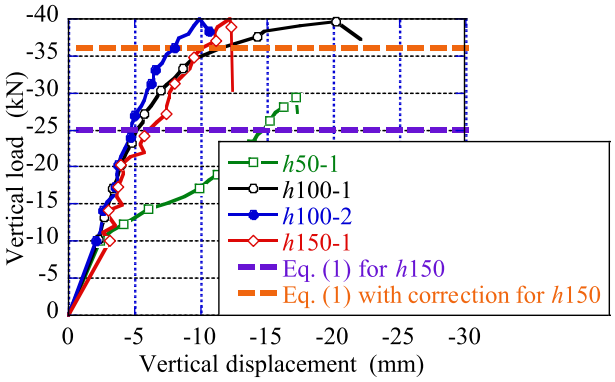

(b) Push-in tests

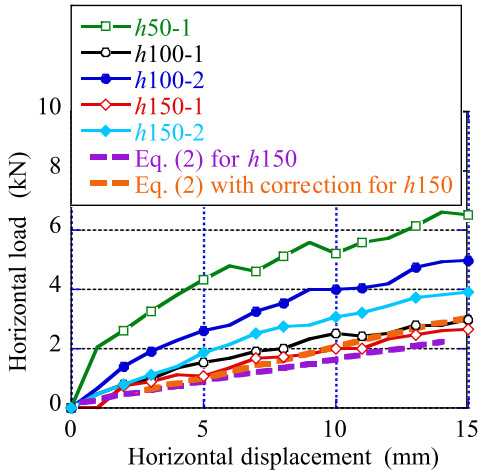

(c) Horizontal loading tests

Fig. 3. Loading test results.

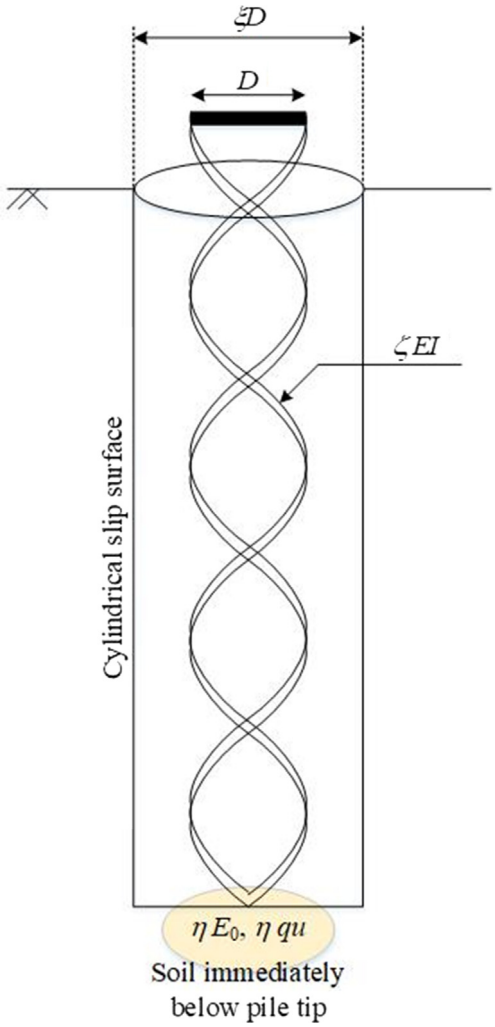

Fig. 4. Influence of integration effect.

$$\beta' = \left(k'_h D' 4EI'\right)^{1/4} = \left(\alpha E_0 \xi^{-3/4} \xi D 4 \zeta EI\right)^{1/4} \quad (6)$$

where R_u: the vertical ultimate bearing capacity (kN), q_p: the ultimate bearing capacity of the ground at the pile tip (kN/m^2), A_p: the area of the pile tip (m^2), ι_c: the peripheral frictional force (kN/m^2), L_c: the thickness of the layer for which peripheral frictional force is considered (m), ϕ: the length of the pile circumference (m), y_t: the horizontal displacement of the pile head (m), β: the characteristic value of the foundation (m^{-1}), h: the pile protrusion length (m), EI: the flexural rigidity of the pile (kN-m^2), H: the horizontal load (kN), M: the pile head moment (kN-m), A_p': the corrected pile tip area (m^2), q_p': the corrected ultimate bearing capacity of the ground at the pile tip (kN/m^2), ϕ': the corrected pile peripheral length (m), β': the corrected characteristic value of the foundation (m^{-1}), q_u: the uniaxial compressive strength (kN/m^2), N: the N value converted by a Swedish sounding test, k_h': the corrected coefficient of horizontal subgrade reaction force (kN/m^3), and αE_0: the deformation modulus of the ground (kN/m^2).

4. REPRODUCTION analysis

In this study, the 3D elastoplastic finite element analysis code "DBLEAVES", developed by Ye et al. (2007), was used to conduct the analysis corresponding to the above-described loading tests and to evaluate the bearing capacity of spiral piles subjected to combined loads. In this repro-

duction analysis, a spiral pile with a complicated shape was simplified into a model using the skeleton-beam type hybrid element proposed by Zhang et al. (2000), and verified for usefulness by Danno and Kimura (2009), as shown in Fig. 5. The features of this model are as follows: (1) The volume of the pile is expressed by setting the parameters so that 90 % of the flexural rigidity of the actual pile is distributed to the beam element of the pile core, and the remaining 10 % is distributed to the solid elements that make up the pile body; thus, the interaction between the pile and the ground can be expressed accurately. (2) A bilinear elastoplastic beam element is used for the beam element of the pile core, according to the Specifications for Highway Bridges, and the full plastic moment of the pile is set based on the yield stress of SS400 steel; thus, the bending failure of the pile can be expressed. (3) By providing a rigid beam element set between the pile core and the constituent nodes, the volume effect of the pile with respect to the vertical load can be properly considered. These characteristics make it possible to express the interaction between the pile and the ground by considering the volume of the pile without losing the variety of expressions or the simplicity of the deformation calculation of the pile by using the beam element. Therefore, it is possible to analyse the deformation of piles in multiple loading directions using one unified model. The correction coefficients discussed in the above section are considered in the determination of the model dimensions and parameters in this analysis. Table 2 shows the parameters used in the analysis.

The Drucker-Prager model, which is the simplest elastoplastic constitutive criterion, was used as the constitutive criterion for the ground, considering that the information on the ground is only the converted N value and that the detailed information may be insufficient. The deformation coefficient E_s of the ground was obtained by using the converted N value and the following equation:

$$E_s = 700N \tag{7}$$

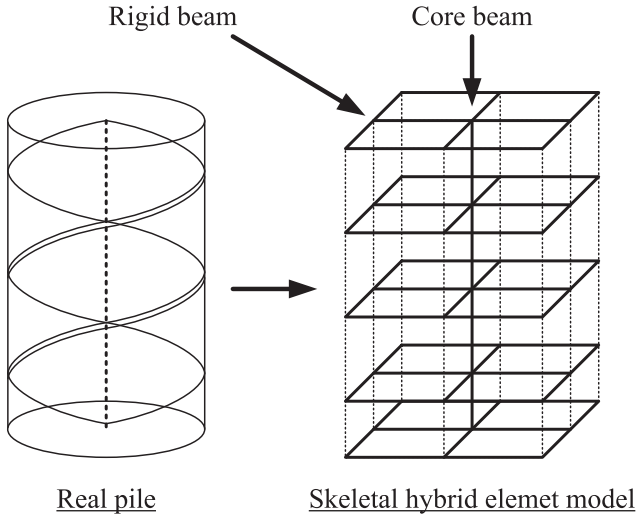

Fig. 5. Skeleton-beam type hybrid element.

The shear strength was calculated by estimating uniaxial compressive strength q_u from the converted N value using Inada's equation, Eq. (4) (Inada 1960), and setting the adhesive strength to 29.25 kPa and the shear resistance angle to 0°. The soil parameters used in the analysis are shown in Table 3.

According to Danno and Kimura (2009), the friction between the pile and the surrounding ground is expressed by the shear deformation of the ground elements around the pile, and the friction between the pile and the ground can be expressed without setting artificial parameters such as joint elements. However, this study aims to analyse not only the push-in load capacity, but also the pull-out load capacity. The judgement was made that it would be difficult to accurately perform the pulling test without using joint elements. Therefore, joint elements were used at the boundary between the pile's peripheral surface and the ground. Since the integration effect of the ground around the pile, due to the rotational press-fitting, leads to an apparent increase in the pile diameter, it can be interpreted that a shear surface generates in the ground. Therefore, a value equal to that of the surrounding ground was used for the shear strength parameter of the joint elements. For the other parameters of the joint elements, various loading test results were taken as reference for determining them. The joint element parameters are summarized in Table 4.

The analysis domain was set as the half-sectional domain shown in Fig. 6 in consideration of the symmetry of the structure and the load used in the tests. The total number of nodes was 8,888, and the number of elements was 7,526. As for the boundary conditions, the displacement was set as free only in the vertical direction for the sides of the domain, and the displacement was set as being constrained in all directions for the bottom of the domain.

Fig. 7 shows a comparison of the results obtained from the numerical analysis and the experiments in **Section 3**. According to this comparison, the numerical analysis can successfully reproduce the experimental results; hence, the validity of the numerical method is confirmed.

5. EVALUATION OF BEARING CAPACITY UNDER COMBINED HORIZONTAL AND VERTICAL loads

In this section, an evaluation of the bearing capacity of the small-diameter spiral pile under the combined horizontal and vertical loads is discussed. The evaluation was conducted by using the parameters established in **Section 4** and the same analysis method used in the identification of these parameters. Fig. 8 shows definitions of the loading point, loading direction, and loading angle. As shown in this figure, the loading point was set at the ground level so that no bending moment would be generated at the pile head. In many cases of the study of piles subjected to combined loads, a constant load is applied in one direction and incremental loading is applied in the other direction (Reddy and Ayothiraman 2015; Lu and Zhang 2018 and so on). In this study, however, both horizontal and vertical loads are

Table 2
Hybrid element parameters.

	Core beam	Solid elements around core beam	Real pile
Section stiffness EA (kN)	$2.12x10^5$	142.0	$2.12x10^5$
Bending stiffness EI (kN-m^2)	3.73	0.42	4.15
Poisson's ratio v	0.30	0.30	0.30
Full plastic moment M_y (kN-m)	17.91	–	17.91

Table 3
Soil parameters.

	Soil	Soil immediately below pile tip
Modulus of deformation E_0 (kPa)	2730	1993
Unit weight γ_t (kN/m^3)	16	16
Poisson's ratio v	0.30	0.30
Adhesive stress c (kPa)	29.25	21.35
Shear resistance angle ϕ (deg)	0	0

Table 4
Joint element parameters.

	Joint	Remarks
Shear stiffness k_s (kN/m)	$1.75x10^5$	Based on loading test results
Normal stiffness k_n (kN/m)	0.14	Based on loading test results
Adhesive stress c_j (kPa)	29.25	Equal to soil
Shear resistance angle ϕ_j (deg)	0	Equal to soil
Tensile strength σ_t (kPa)	2.93	Based on loading test results
Separation judgment value	0.001	Based on loading test results

applied simultaneously by using an inclined load. The analyses were done by changing the loading angle from −90° to 90° in 10° increments; this allowed both the push-in load capacity and the pull-out load capacity to be taken into account.

Fig. 9**(a)** shows the relationship between the vertical load and the vertical displacement for all loading directions. The initial gradient of the vertical load vs vertical displacement does not depend on the loading angle. However, the ultimate bearing capacity of pulling-out (positive loading angle) and that of pushing-in (negative loading angle) increase as the loading direction approaches the vertical direction. It can be noticed from Fig. 9**(a)** that the pushing-in load capacity is higher than the pulling-out load capacity.

Fig. 9**(b)** shows the relationship between the horizontal load and the horizontal displacement for all loading directions. Here, as well, the initial gradient of the horizontal load vs horizontal displacement curve does not depend on the loading angle; the ultimate horizontal capacity for both positive and negative loading angles decreases as the loading direction approaches the vertical direction. The horizontal capacity for the negative loading angle is higher than that for the positive loading angle, especially when the loading direction approaches the vertical direction; this is in concordance with Ashour et al. (2020). This can be explained by the upward soil movement induced in front of the pile when the loading angle is positive, which decreases both the soil strength and the horizontal capacity. On the contrary, when the negative loading angle is applied, the soil in front of the pile undergoes a moderate compaction or confinement which increases both the soil strength and the horizontal capacity.

Fig. 9**(c)** shows the relationship between the loading direction and the displacement direction of the pile head. From Fig. 9**(c)**, it can be understood that the loading direction and the displacement direction agree with each other in the case of $\theta = \pm 90°$. However, in the other cases, the displacement angle is smaller than the loading angle, and the horizontal displacement tends to be predominant. The bending moment generated in the pile does not reach the full plastic moment, and the pile behaves within the elastic range in all cases.

Based on these results, the bearing capacity envelope for the combined horizontal and vertical loads is shown as a blue line with square markers in Fig. 10. Here, the load that is the first to reach the ultimate state, in either the vertical or horizontal direction, is defined as the bearing capacity. In other words, the bearing capacity obtained against combined loading is defined as the load whose vertical or horizontal displacement component reaches 10 %D sooner. The broken black line shows the vertical and horizontal bearing capacities obtained against the pure push-in, pull-out, and lateral loading for reference. From Fig. 10, it can be observed that the ultimate load was reached first in the horizontal direction in the range from −80° to 80°.

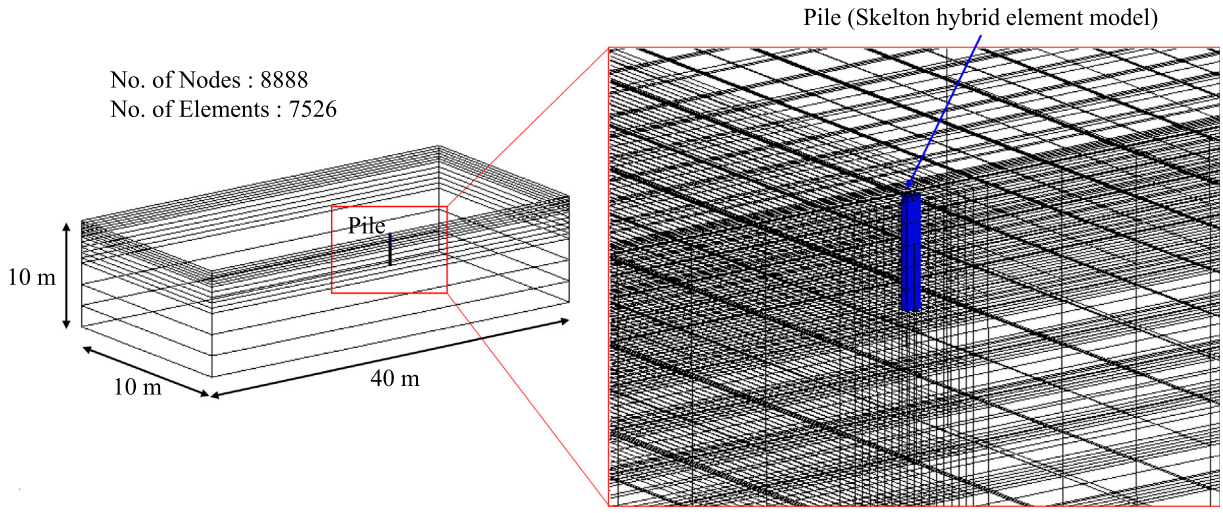

(a) Single vertical pile ($\alpha = 0°$)

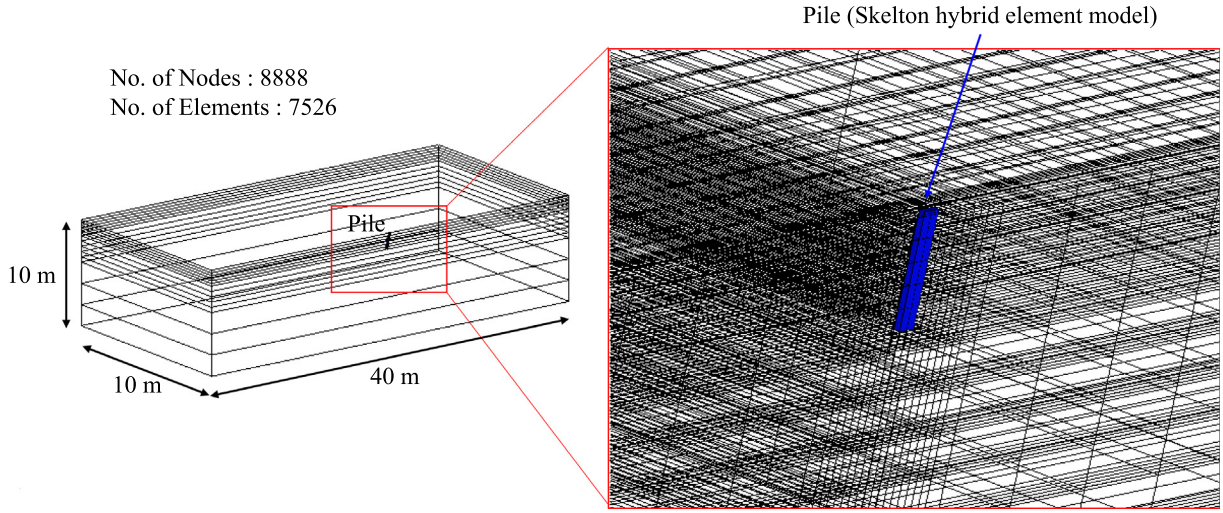

(b) Single batter spiral pile ($\alpha = 30°$)

Fig. 6. Analysis mesh.

The load's inclination does not affect the horizontal response of the vertical pile much; it mainly affects the axial response. This observation is in concordance with Shahrour and Meimon (1991) and Mroueh and Shahrour (2007). The envelope has a vertically long elliptical shape with the centre located below the origin (zero 0) because it exhibits a greater ultimate load in the push-in direction.

From the above, by considering that the load that reaches the ultimate state first, in either the vertical or horizontal direction, is the bearing capacity, the bearing capacity calculated individually against each pure push-in, pull-out, and lateral loading was evaluated as being on the dangerous side against the combined horizontal and vertical loading. In addition, since the resistance in the vertical direction has a relatively greater margin than that in the horizontal direction, it is suggested that piles that have excellent resistance performance in the vertical direction, such as batter piles, should be investigated. The following findings were obtained from the above examinations.

(1) The resistance in the vertical direction has a relatively greater margin than the resistance in the horizontal direction.
(2) The ultimate bearing capacity obtained independently for each loading direction is evaluated on the dangerous side with respect to the bearing capacity under the combined loads.
(3) The pushing-in load capacity is higher than the pulling-out resistance.

Under the same analysis conditions, a series of analyses was performed considering the moment load (M) and the

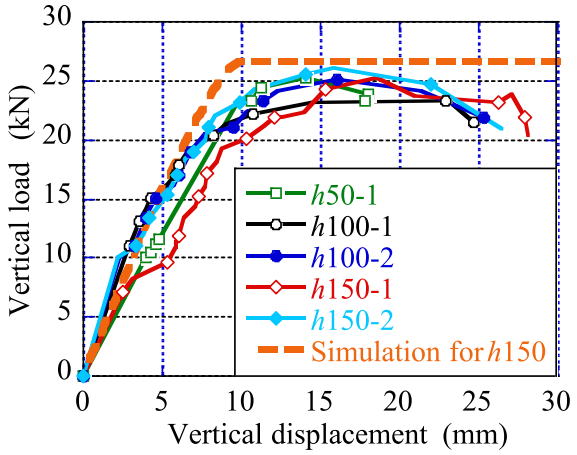

(a) Pull-out tests

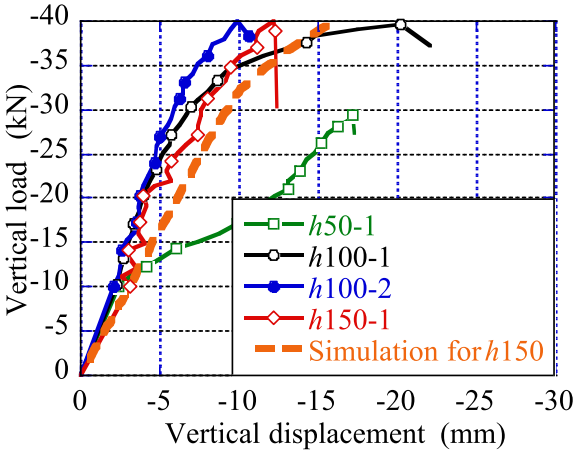

(b) Push-in tests

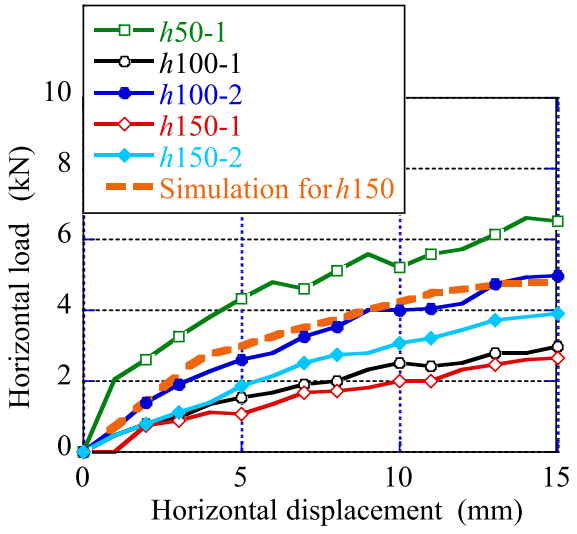

(c) Horizontal loading tests

Fig. 7. Numerical simulation results with loading test results.

bearing capacity characteristics of the spiral pile for the *H-V-M* combined loads investigated. In this analysis, the standard location of the centre of the mass of the superstructure of a photovoltaic power generation facility was assumed to be 1.5 m from the ground surface, and the value obtained by multiplying this by horizontal load H was applied to the loading point as the moment load. In addition, as the numerical experiments, analyses were performed in which the location of the centre of the mass of the superstructure (equivalent to the loading height mentioned in section 2) was changed to h = 3.0 m and h = 5.0 m, and the bearing capacity characteristics for the *H-V-M* combined loads were obtained.

Fig. 11 shows the bearing capacity curve of the spiral pile under the combined loads. As in the previous section, the bearing capacity is defined as the load that leads to the ultimate state first, in either the vertical or horizontal direction (i.e., the load when the displacement reaches 10 mm, 10 % of the pile diameter). From this figure, the horizontal resistance significantly decreases when moment load M is applied, and the bearing capacity envelope is scaled down in the horizontal direction compared to the case without moment load M (i.e., where h = 0 m). Based on these results, a formula has been proposed for estimating the bearing capacity of a spiral pile under *H-V-M* combined loads in the next section.

6. FORMULA FOR ESTIMATING BEARING CAPACITY OF VERTICAL SPIRAL PILE UNDER COMBINED loads

From the bearing capacity characteristics of the spiral pile under the *H-V-M* combined loads discussed in the previous section, the bearing capacity envelope is depicted as a conceptual diagram in the *H-V-M* space, as shown in Fig. 12**,** and can be expressed by **Eq. (8)**. When this is projected onto the *H-V* space, it is expressed by **Eq. (9)**.

$$\left(\frac{H}{H_{\pm}}\right)^2+\left(\frac{V}{V_{\pm}}\right)^2+\left(\frac{M}{M_{\pm}}\right)^2=1 \tag{8}$$

$$\left(\frac{H'}{H'_{\pm}}\right)^2+\left(\frac{V}{V_{\pm}}\right)^2=1 \tag{9}$$

$$H'_{\pm}=\frac{a|_{h=0}}{a+bh}H_{\pm}=\frac{3}{5(\psi\beta'\eta)^3+12(\psi\beta'h)^2+9\psi\beta'h+3}H_{\pm} \tag{10}$$

$$M_{\pm}=hH'_{\pm}=\begin{cases}\frac{3h}{5(\beta h)^3+12(\beta h)^2+9\beta h+3}H_{\pm} \text{ in case of } & 0\leqslant\tan^{-1}\left(\frac{M}{H}\right)<\frac{\pi}{2}\\ M_{\pm} \text{ in case of } & \tan^{-1}\left(\frac{M}{H}\right)=0\end{cases} \tag{11}$$

V_+ and V- represent the pull-out (positive) and push-in (negative) bearing capacities in the direction of the pile axis, respectively, and H_+, M_+ and H_-, M_- represent the horizontal and moment load capacities with respect to the positive and negative load directions in Fig. 8. $H'_{\pm}$ is the horizontal bearing capacity when a moment load is applied. a and b are the coefficients of the first and second

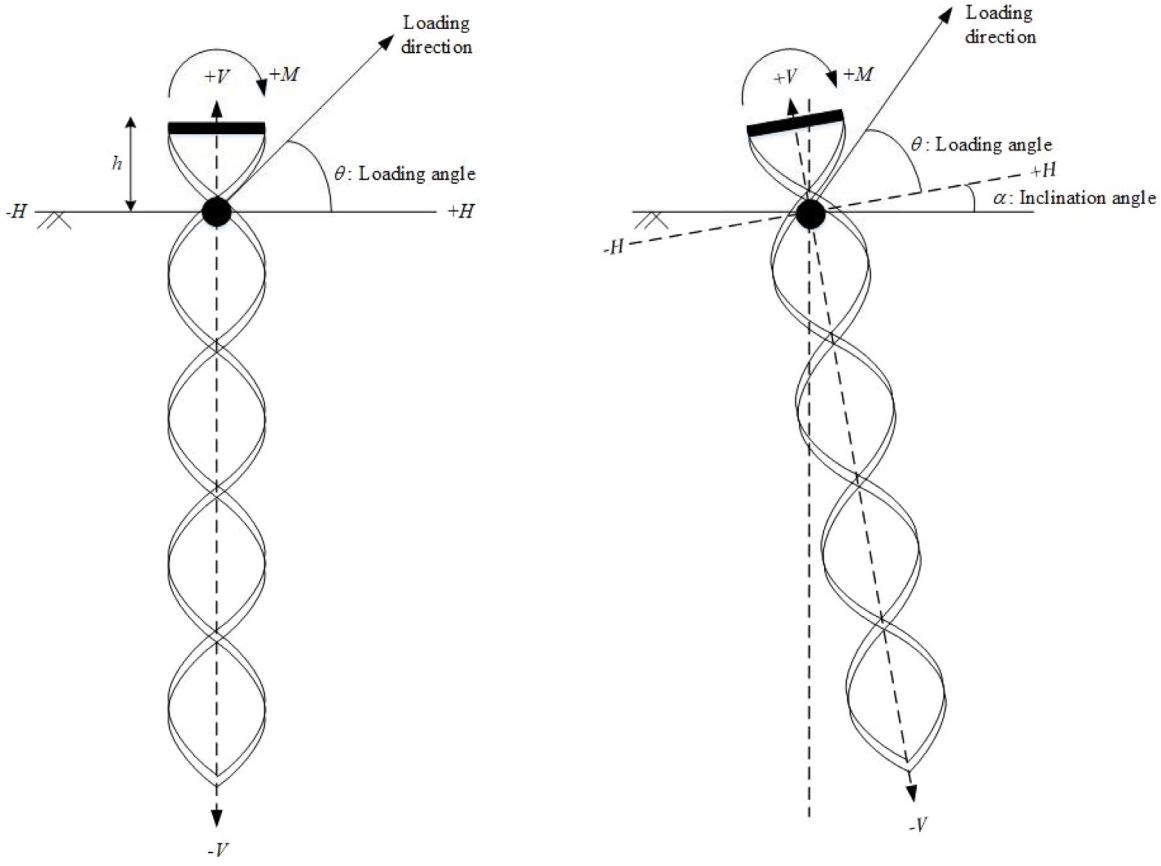

(a) Vertical pile (b) Batter pile

Fig. 8. Definitions of loading point, loading direction, and loading angle of combined loads.

terms in Chang's equation (**Eq. (2)**), which are functions of h. ψ is a correction coefficient used to consider the influence under the ultimate state, which β' in **Eq. (6)** does not consider sufficiently, because it is determined based on Chang's equation, which models the elastic behavior of a uniform ground along depth. The characteristic of these estimation formulas is that, if the bearing capacities in the direction of the pile axis and the direction perpendicular to the pile axis can be obtained by a loading test, the bearing capacity of the pile under the *H-V-M* combined loads can be estimated. However, further numerical simulation and loading tests are necessary because the correction coefficient also depends on the pile size, spiral shape, and characteristics of the surrounding ground.

In Fig. 13, the numerically obtained and the estimated bearing capacity values are compared for the combined loads when $h = 0.0$ m and $h = 1.5$ m. From this figure, it is confirmed that the estimation formulas can evaluate the analysed values with high accuracy. The coefficients of determination were calculated to verify the accuracy and are shown in Table 5. From this table, it is seen that the accuracy of the estimated values is extremely high when loading height h is low, but the estimation accuracy tends to decrease when the loading height is high. Therefore, to improve the accuracy of the estimation formulas, it will be necessary to carry out further verification using a comprehensive approach, including model and field experiments.

7. BEARING CAPACITY CHARACTERISTICS OF BATTER SPIRAL PILES UNDER COMBINED loads

Using the same analysis method as described in the above sections, loading analyses were performed to clarify the characteristics of the bearing capacity of batter spiral piles when combined loads were applied. Six series of analyses were performed by changing the inclination angle α (from the vertical direction) of the pile every 5° up to the applicable angle of 30° for lightweight piles. The loading conditions, loading point, and analysis parameters were not changed from those of the vertical piles. For the batter piles, however, the range in loading directions (angles) was from −180° to 180°. This range was set by considering that batter piles exhibit asymmetrical bearing capacity characteristics for the loading direction. In this study, by changing the loading angle from −180° to 180°, the capacity of both the negative and positive batter piles, defined by the

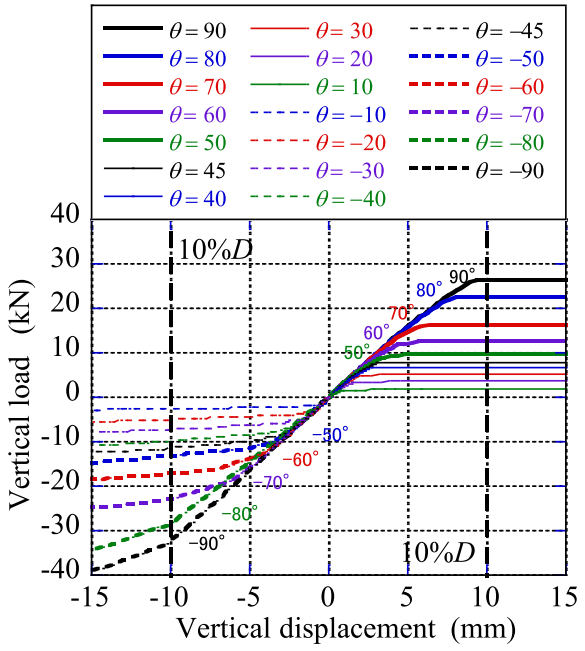

(a) Vertical load vs. vertical displacement

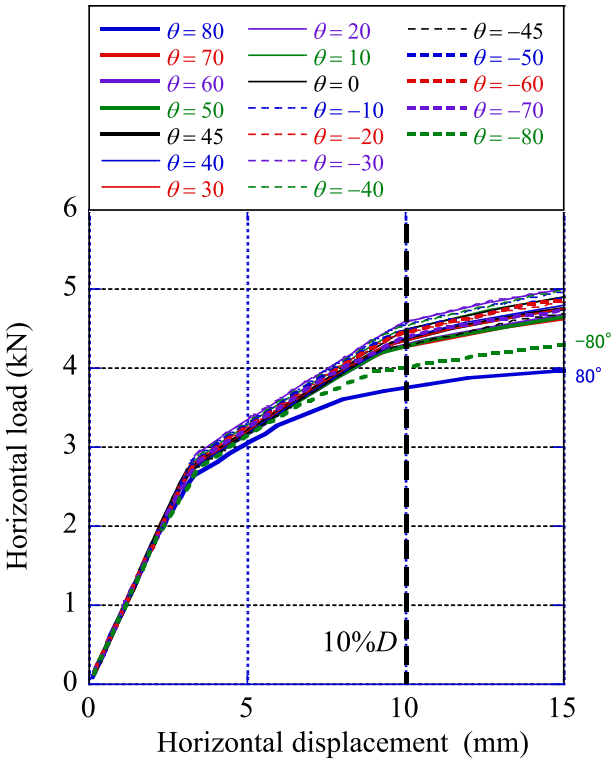

(b) Horizontal load vs. horizontal displacement

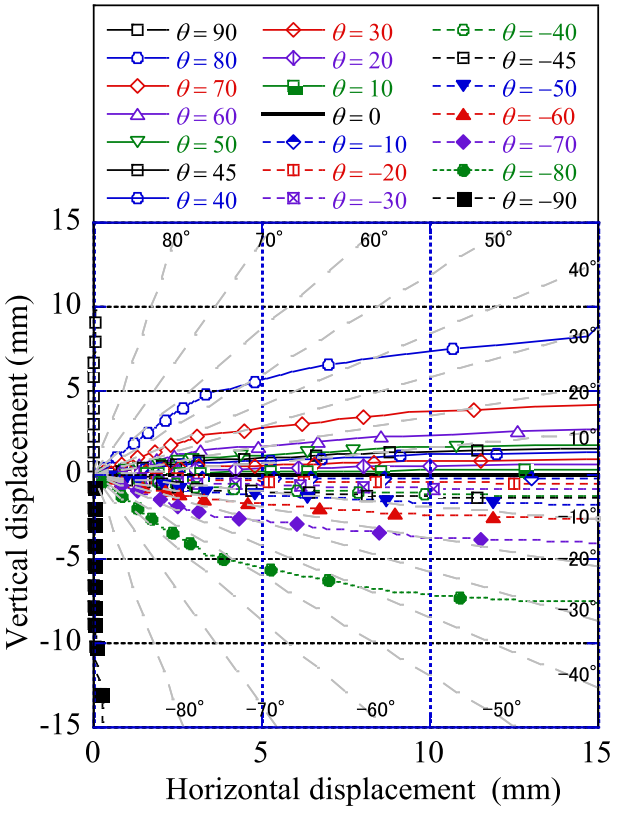

(c) Loading direction vs. displacement direction

Fig. 9. Numerical simulation results for spiral pile subjected to combined loads.

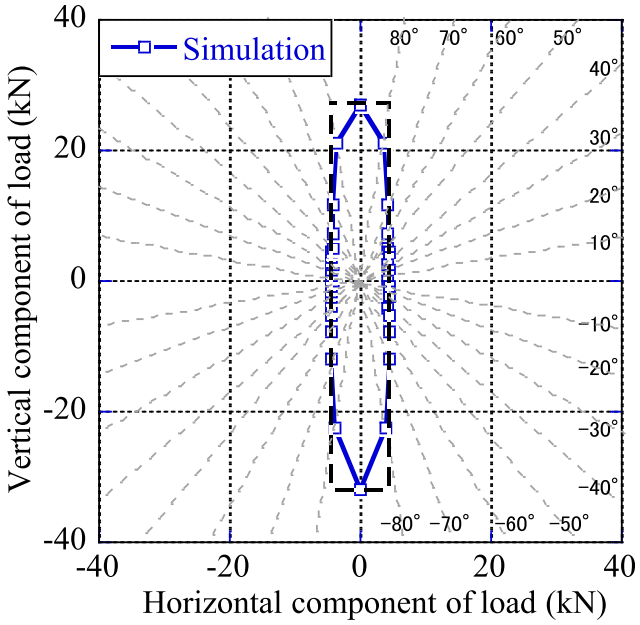

Fig. 10. Bearing capacity envelope of spiral pile for combined loads (*H-V*).

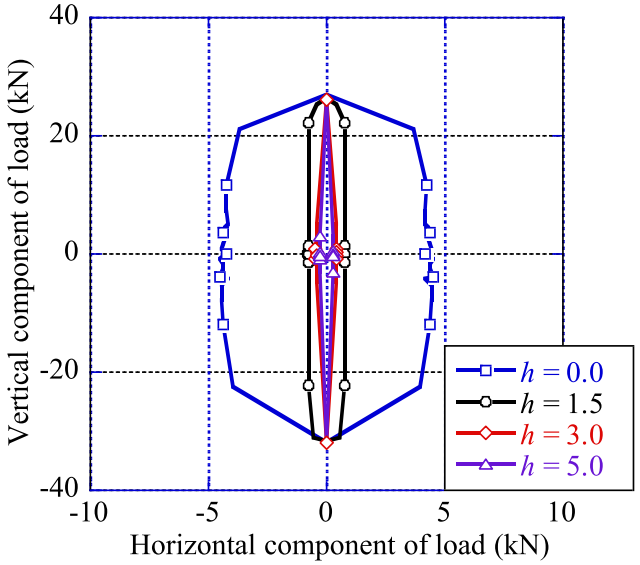

Fig. 11. Bearing capacity envelope for combined loads (*H-V-M*) of vertical pile.

relationship between the loading direction and the pile inclination direction, could be investigated.

Fig. 14 shows the bearing capacity envelopes of batter spiral piles under combined loads. As in the previous section, the bearing capacity is defined as that of the load that arrives at the ultimate state first in either the vertical or horizontal direction (i.e., the load when the displacement reaches 10 mm, 10 % of the pile diameter). Compared with Fig. 10, it can be seen that the bearing capacity envelopes of the batter spiral piles show elliptical shapes in which the pile axis direction of the batter piles is the major axis direction. This shape is in an agreement with the shape

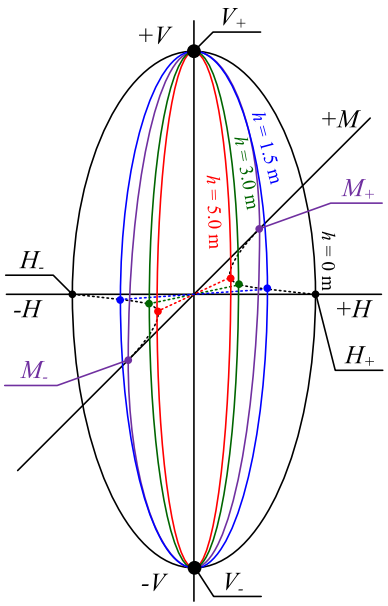

Fig. 12. Conceptual diagram of bearing capacity envelope for *H-V-M* combined loads.

obtained by Mroueh and Shahrour (2009) who studied the response of battered piles to inclined pull-out loads. The pull-out and push-in capacities both decrease when batter angle α increases.

From the characteristics of the bearing capacity of the batter spiral piles under the combined loads, the bearing capacity envelopes of the small-diameter spiral piles under combined loads can be formulated by the following equations:

$$\left(\frac{H^*}{H^*_+}\right)^2 + \left(\frac{V^*}{V^*_+}\right)^2 = 1 \tag{12}$$

$$\left(\frac{H^*}{H^*_-}\right)^2 + \left(\frac{V^*}{V^*_+}\right)^2 = 1 \tag{13}$$

$$\left(\frac{H^*}{H^*_-}\right)^2 + \left(\frac{V^*}{V^*_-}\right)^2 = 1 \tag{14}$$

$$\left(\frac{H^*}{H^*_+}\right)^2 + \left(\frac{V^*}{V^*_-}\right)^2 = 1 \tag{15}$$

$$\begin{pmatrix} H^* \\ V^* \end{pmatrix} = \begin{bmatrix} \cos\alpha & -\sin\alpha \\ \sin\alpha & \cos\alpha \end{bmatrix} \begin{pmatrix} H \\ V \end{pmatrix} \tag{16}$$

H^* and V^* are the horizontal and vertical loads, respectively, after the coordinate transformation by the rotation matrix using the inclination angle α of the batter pile. They are expressed by **Eq. (16)**. V^*_+ and V^*_- represent the pull-out (positive) and push-in (negative) bearing capacities in the direction of the pile axis, respectively, H^*_+ represents the bearing capacity when the loading is applied perpendicular to the pile axis on the inclined side of the pile, and H^*_- represents when the loading is done in the reverse direction to that for H^*_+. Therefore, **Eq. (12)** represents the case where the loading is in the direction of the first quadrant

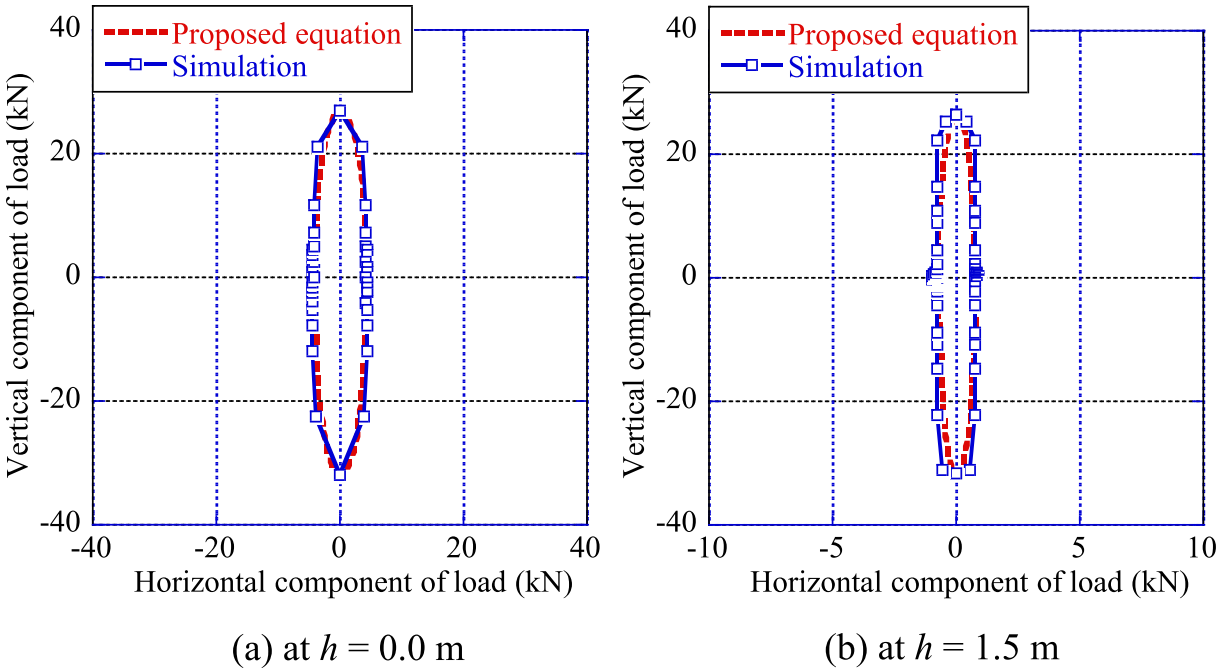

Fig. 13. Comparison of estimated and analysis values.

Table 5
Verification of accuracy of estimated values for vertical spiral pile subjected to combined loads (*H-V-M*).

h (m)	0	1.5	3	5
R^2	0.99	0.54	0.68	0.65

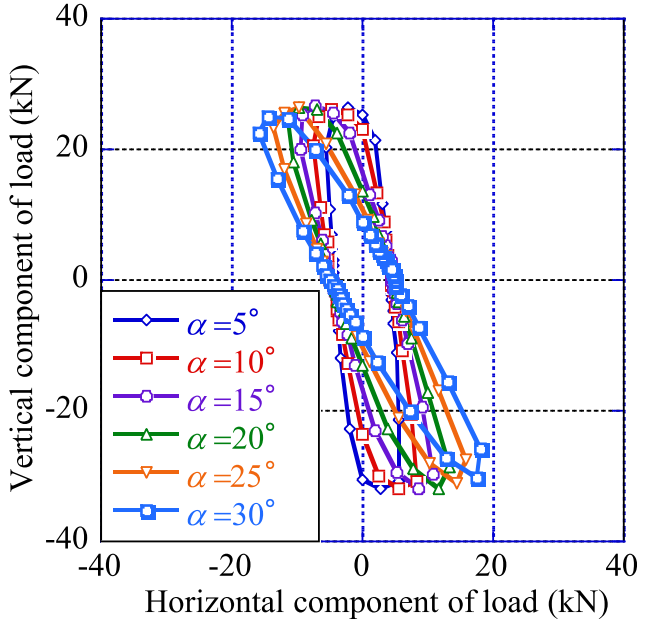

Fig. 14. Bearing capacity envelopes of batter spiral piles under combined loads.

after the coordinate transformation, and **Eq. (14)** represents the case where the loading is in the direction of the third quadrant. An illustration of the equations is given in Fig. 15.

Fig. 16 provides a comparison of the numerical and analytically estimated values of the bearing capacity under the combined loads when the batter angle was 15° and 30°. In these cases, loading height *h* was 0 m. From this figure, it can be verified that the evaluated values accurately represent the numerically analysed values for both batter angles. The coefficients of determination were calculated to verify the accuracy and are shown in Table 6. The coefficient of determination is 0.97 or higher for each of the cases with different batter angles. This demonstrates that the proposed estimation equations are able to evaluate the bearing capacity of spiral piles under combined loads with extremely high accuracy. The above indicates that, if the bearing

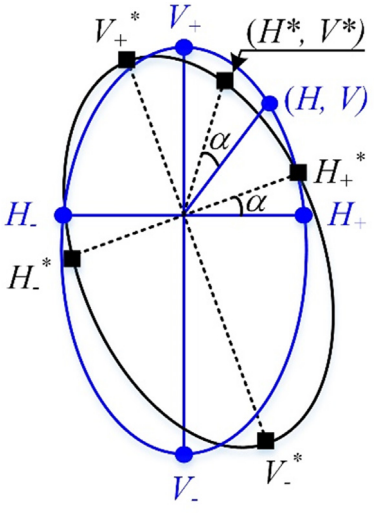

Fig. 15. Schematic view of proposed equations (12) through (16).

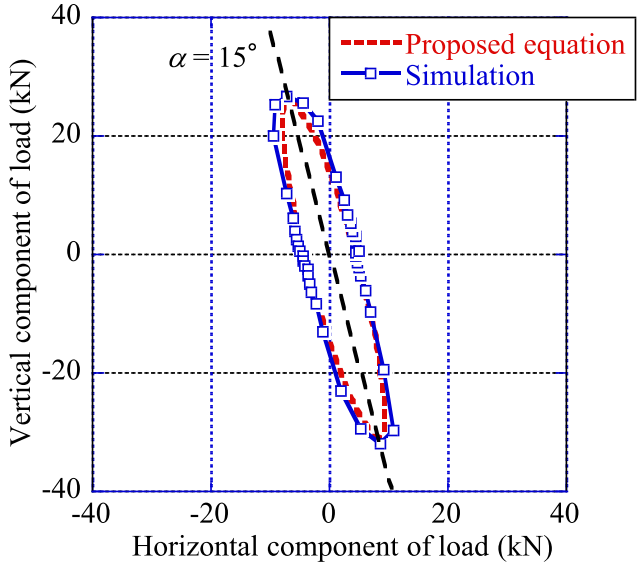

(a) for $\alpha = 15^{\circ}$

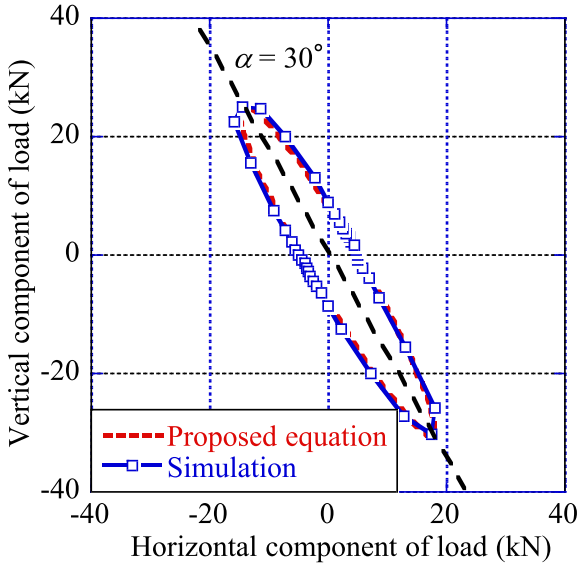

(b) for $\alpha = 30^{\circ}$

Fig. 16. Comparison of estimated and analysis values ($h = 0$).

Table 6
Verification of accuracy of estimated values for batter spiral pile subjected to combined loads (H-V) with loading height h of 0 m.

α (deg)	0	5	10	15	20	25	30
R^2	0.99	0.97	0.99	0.99	0.99	0.99	0.98

capacity in the direction of the pile axis and that perpendicular to the pile axis can be obtained by a loading test, the bearing capacity under combined load can be accurately evaluated by these estimation formulas. Therefore, the high degree of usefulness of the formulas is demonstrated.

For more reliability, the proposed equations are compared with the existing literature (Mroueh and Shahrour, 2009), in which a three-dimensional finite element analysis was used to investigate the response of batter piles against the combined horizontal and vertical pull-out loads, while considering the nonlinear behaviour of dry medium dense sand. Fig. 17 shows a comparison of the failure envelopes for three batter angles of $\alpha = 0$ (vertical pile), -10, and $-20°$. Loading height h was 0 m. From this figure, it can be seen that the proposed formulas match pretty well with the results of Mroueh and Shahrour (2009), although the failure envelopes from the proposed formulas are slightly thinner. The slight discrepancy might be caused by the fact that the proposed formulas were established based on the simulation results for small-diameter spiral piles in clay, assuming a cylindrical shape of the slip surface around each pile. Therefore, further investigations will be necessary for other types of soils.

8. Summary

The findings obtained from the results of various loading tests on small-diameter spiral piles and the three-dimensional elastoplastic finite element analysis for evaluating the bearing capacity for combined loads are summarized below.

(1) Integration effect between spiral pile and the surrounding ground derived from rotational press-fitting.

The integration effect between each rotationally press-fit spiral pile and the surrounding ground was considered in a simple way. To appropriately reflect the integration effect derived between the rotationally press-fit pile and the sur-

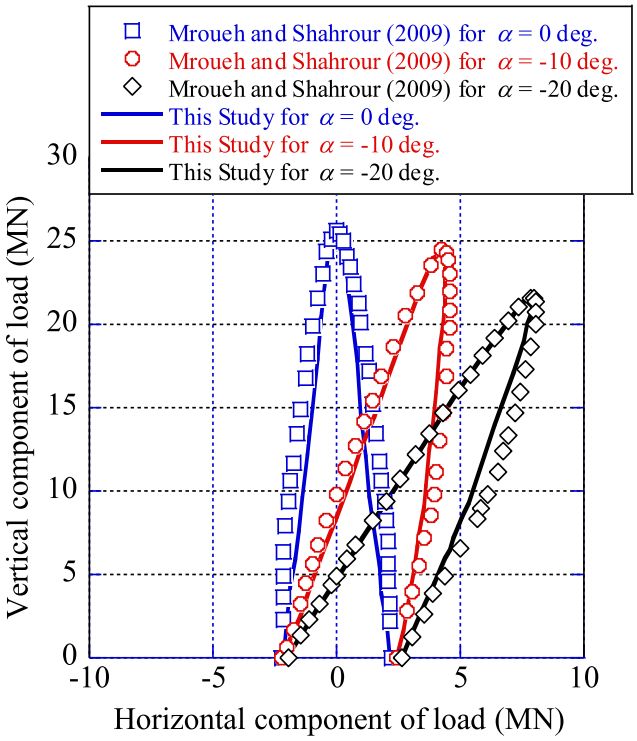

Fig. 17. Comparison with Mroueh and Shahrour (2009).

rounding ground, corrections were done on the elements, such as increasing the apparent pile diameter, increasing the strength of the ground immediately below the pile tip, and increasing the bending rigidity of the pile. As a result, a high integration effect in both positive and negative vertical directions could be confirmed.

(2) Reproduction analysis results of various loading tests.

The experimental results were accurately expressed in each case by modelling the complex shape of the spiral pile and the integration effect on the surrounding ground by rotational press-fitting. In this modelling, the skeleton beam-type hybrid element, that takes into account the correction coefficients discussed in (1), was incorporated.

(3) Bearing capacity characteristics of straight and batter spiral piles under combined loads.

It was shown that the bearing capacity under combined loads might be lower than the bearing capacity evaluated independently for the vertical and horizontal loading, depending on the loading direction. In other words, it is possible that the ultimate bearing capacity is evaluated on the dangerous side when using the conventional design method.

(4) Bearing capacity estimation formula for combined loads.

The bearing capacity envelopes were formulated in this study for small-diameter spiral piles under the *H-V-M* combined loads, formulas were proposed for estimating the bearing capacity of these spiral piles, and the estimation accuracy of the formulas was verified. As a result, it was confirmed that the proposed estimation formulas can estimate the bearing capacity curves of *H-V-M* combined loads of spiral piles with high accuracy for each of the set inclination angles. Therefore, if the bearing capacity in the direction of the pile axis and that perpendicular to the pile axis can be obtained by a loading test, the bearing capacity under the combined loads can be evaluated accurately by these estimation formulas. The accuracy of the estimated values is extremely high when loading height h is low, but the estimation accuracy tends to decrease as loading height h increases. Therefore, to improve the accuracy of the estimation formulas, it will be necessary to carry out further verification in the future, using a comprehensive approach that includes model and field experiments.

Acknowledgements

This work was partially supported by JSPS KAKENHI Grant Number 20K04678 and JST SPRING, Grant Number JPMJSP2119.

References

Abdel-Rahman, K., Achmus, M., 2006. Numerical modelling of the combined axial and lateral loading of vertical piles. Numer. Meth. Geotech. Eng., 575–581

Achmus, M., Thieken, K., 2010. On the behavior of piles in non-cohesive soil under combined horizontal and vertical loading. Acta Geotech. 5 (3), 199–210.

Araki, K., 2013. Simple foundation method subject to small-scale structures "Pin Foundation Method". J. Geotech. Eng. 61 (8), 32–33, in Japanese.

Ashour, M., Alaaeldin, A., Arab, M.G., 2020. Laterally Loaded Battered Piles in Sandy Soils. J. Geotech. Geoenviron. Eng. 146 (1), 06019017.

Ayothiraman, R., Reddy, K.M., 2014. Model experiments on pile behaviour in loose-medium dense sand under combined uplift and lateral loads. Tunn. Undergr. Constr. GSP 242, 633–643.

Danno, K., Kimura, M., 2009. Evaluation of long-term displacements of pile foundation using coupled FEM and centrifuge model test. Soils Found. 49 (6), 941–958.

Darr, K.A., Reese, L.C., Wang, S.T., 1990. Coupling effects of uplift loading and lateral loading on capacity of piles. Offshore Technology Conference, British Maritime Technology Teddington, 443–450.

Das, B.M., Raghu, D., Seeley, G.R., 1976. Uplift capacity of model piles under oblique loads. J. Geotech. Eng. Div. 102 (9), 1009–1013.

Gotman, A.L., 2000. Finite-element analysis of tapered piles under combined vertical and horizontal loadings. Soil Mech. Found. Eng. 37 (1), 5–12.

Hirata, A., Kokaji, S., Seung, K.S., Goto, T., 2005. Study on the Estimation of the Axial Resistance of Spiral Bar Based on Interaction with Ground. Shigen to Sozai. 121 (8), 370–377.

Inada, M., 1960. About the use of Swedish sounding test results. Soil Mech. Found. Eng. 8 (1), 13–18, in Japanese.

Ismael, N.F., 1989. Field tests on bored piles subject to axial and oblique pull. J. Geotech. Eng. 115 (11), 1588–1598.

Jain, N.K., Ranjan, G., Ramasamy, G., 1987. Effect of vertical load on flexural behaviour of piles. Geotech. Eng. 18 (2), 185–204.

Japanese Geotechnical Society, 2004. Method for static axial compressive load test of single Piles. [JGS 1811-2002].

Japanese Geotechnical Society, 2004. Method for Static Axial Tensile Load Test of Single Piles. [JGS 1813-2002].

Japanese Geotechnical Society, 2010. Method for lateral load test. [JGS 1831-2010].

Johnson, K., 2005. Load–deformation behaviour of foundations under vertical and oblique load. James Cook University, Australia, Ph.D. thesis.

Karthigeyan, S., Ramakrishna, V.V.G.S.T., Rajagopal, K., 2006. Influence of vertical load on the lateral response of piles in sand. Comput. Geotech. 33 (2), 121–131.

Karthigeyan, S., Ramakrishna, V.V.G.S.T., Rajagopal, K., 2007. Numerical investigation of the effect of vertical load on the lateral response of piles. J. Geotech. Geoenviron. Eng. 133 (5), 512–521.

Lu, W., Zhang, G., 2018. Influence mechanism of vertical-horizontal combined loads on the response of a single pile in sand. Soils Found. 58 (5), 1228–1239.

Meyerhof, G.G., 1981. The bearing capacity of rigid piles and pile groups under inclined load in clay. Can. Geotech. J. 18 (2), 297–300.

Meyerhof, G.G., Yalcin, A.S., Mathur, S.K., 1983. Ultimate pile capacity for eccentric inclined load. J. Geotech. Eng. 109 (3), 408–423.

Mroueh, H., Shahrour, I., 2007. Response of piles to inclined uplift loads: Influence of the soil-pile interface. Eur. J. Comput. Mech. 16 (3–4), 419–435.

Mroueh, H., Shahrour, I., 2009. Numerical analysis of the response of battered piles to inclined pullout loads. Int. J. Numer. Anal. Meth. Geomech. 33 (10), 1277–1288.

Rao, S.N., Prasad, Y.V.S.N., 1993. Uplift behavior of pile anchors subjected to lateral cyclic loading. J. Geotech. Eng. 119 (4), 786–790.

Reddy, M.K., Ayothiraman, R., 2015. Experimental Studies on Behavior of Single Pile under Combined Uplift and Lateral Loading. J. Geotech. Geoenviron. Eng. 141 (7), 04015030.

Sato, T., Harada, T., Iwasa, N., Hayashi, S., Otani, J., 2015. Effect of shaft rotation of spiral piles under its installation on vertical bearing capacity. Jpn. Geotech. J. 10 (2), 253–265, in Japanese.

Shahrour, I., Meimon, Y., 1991. Analysis of the behaviour of offshore piles under inclined loads. Int. Conf. Deep Found., 277–284
Shanker, K., Basudhar, P.K., Patra, N.R., 2007. Uplift capacity of single piles: Predictions and performance. Geotech. Geol. Eng. 25 (2), 151–161.
Small, J.C., Zhang, H.H., 2002. Behavior of piled raft foundations under lateral and vertical loading. Int. J. Geomech. 2 (1), 29–45.
Suits, L.D., Sheahan, T.C., Puppala, A.J., Wejrungsikul, T., Williammee, R.S., Thomas Witherspoon, W., Lozano, N., 2012. Inclined tensile load testing on short drilled shafts. Geotech. Test. J. 35 (2), 103343.
Suleiman, M.T., Vande Voort, T., Sritharan, S., 2010. Behavior of driven ultrahigh-performance concrete H-piles subjected to vertical and lateral loadings. J. Geotech. Geoenviron. Eng. 136 (10), 1403–1413.
Ye, B., Ye, G., Zhang, F., Yashima, A., 2007. Experiment and numerical simulation of repeated liquefaction consolidation of sand. Soils Found. 47 (3), 547–558.
Zhang, H.H., Small, J.C., 2000b. Analysis of capped pile groups subjected to horizontal and vertical load. Comput. Geotech. 26 (1), 1–21.
Zhang, F., Kimura, M., Nakai, T., Hoshikawa, T., 2000. Mechanical Behavior of Pile Foundations Subjected to Cyclic Lateral Loading Up to the Ultimate State. Soils Found. 40 (5), 1–17.